Supporting Information

Robust FeCoP Nanoparticles Grown on rGO-Coated Ni Foam as An Efficient Oxygen Evolution Catalyst for Excellent Alkaline and Seawater Electrolysis

Yingping Zheng [a,b], Dehua Yu [a], Wei Xu [b], Ke Zhang [a], Kaili Ma [b], Xinyu Guo [a], Yongbing Lou [,a] and Mulin Hu [*,c]*

[a] School of Chemistry and Chemical Engineering, Southeast University, Nanjing, 211189, P. R. China. E-mail: lou@seu.edu.cn.

[b] Analysis and Testing Center, Southeast University, Nanjing 211189, P. R. China.

[c] Hefei Technology College, Hefei 238000, P. R. China.

***Email(s):** lou@seu.edu.cn (Prof. Yongbing Lou).

List of Figures and Tables

Pretreatment of NF.

Inevitably, there would be oxides and impurities in the process of nickel foam production, transportation and storage. Hence, ultrasonic cleaning was first conducted in 3 M HCl for 15 min to eliminate their influence. Then nickel foam followed by repeated rinsing with deionized water and absolute ethanol to remove excess acid. Last, this cleaned NF was dried in a vacuum oven for further usage.

Pretreatment of rGO.

This process was divided into three steps, low temperature, medium temperature and high temperature. Low-temperature reaction. After adding 7 mL concentrated sulfuric acid into a clean and dry 100 mL round bottom flask, it was put into an ice-water bath keeping the temperature at 0 °C. 0.3 g graphite powder was added into the concentrated sulfuric acid with magneton stirring, then 0.9 g potassium permanganate was added in batches while the reaction temperature was controlled below 20 °C. Medium temperature reaction. After removing the ice-water bath, the flask was heat up to 40 °C, and continue stirring for 30 min. The color of the solution turns brown-black. High temperature reaction. 15 mL deionized water was slowly added into the brown-black solution, then the temperature was raised to 95 °C and kept for 15 min. Finally, 50 mL deionized water was added continuously before 1.5 mL 30 % hydrogen peroxide was slowly added. The color of the aqueous solution became bright yellow. After centrifugation, the yellow solid was washed repeatedly with 5% dilute hydrochloric acid and deionized water, and the final viscous yellow gel was GO.

Pretreatment of FeCoP@rGO/GCE.

For comparison, a general method was used to coat FeCoP@rGO catalyst on glassy carbon electrode (GCE). Typically, a homogeneous ink was obtained by dispersing 4 mg FeCoP@rGO powder and 30 μL Nafion solution (5.0 wt.%) into 1 mL 50 % alcohol solvent after 0.5 h sonication. Then, the above ink was coated on the GCE and dried

naturally. Thus, FeCoP@rGO/GCE electrodes were prepared.

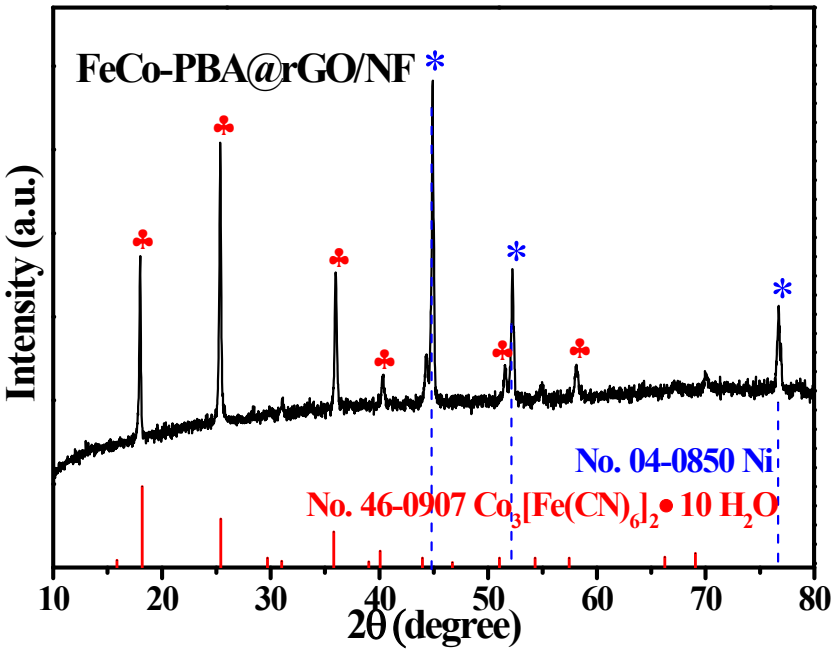

Figure S1. XRD patterns of FeCo-PBA@rGO/NF.

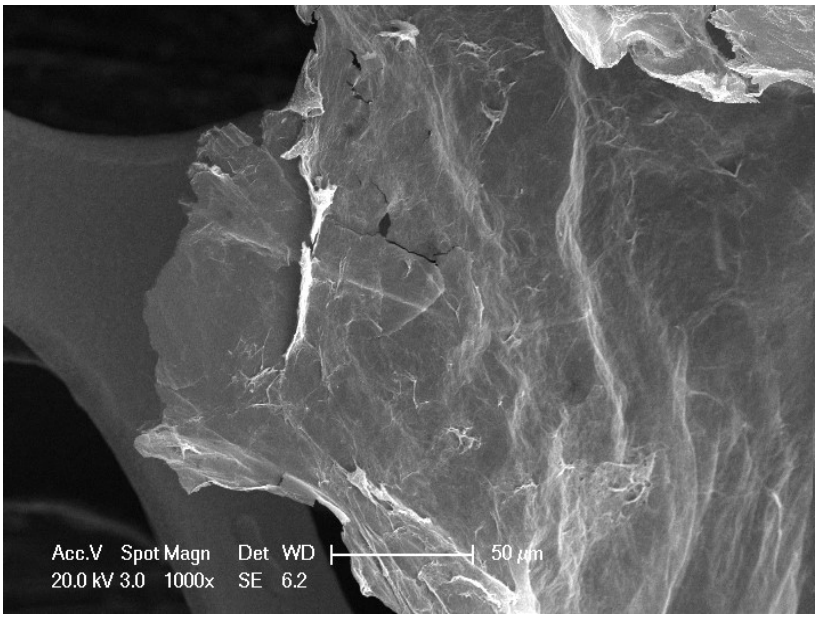

Figure S2. SEM images of rGO-coated Ni foam.

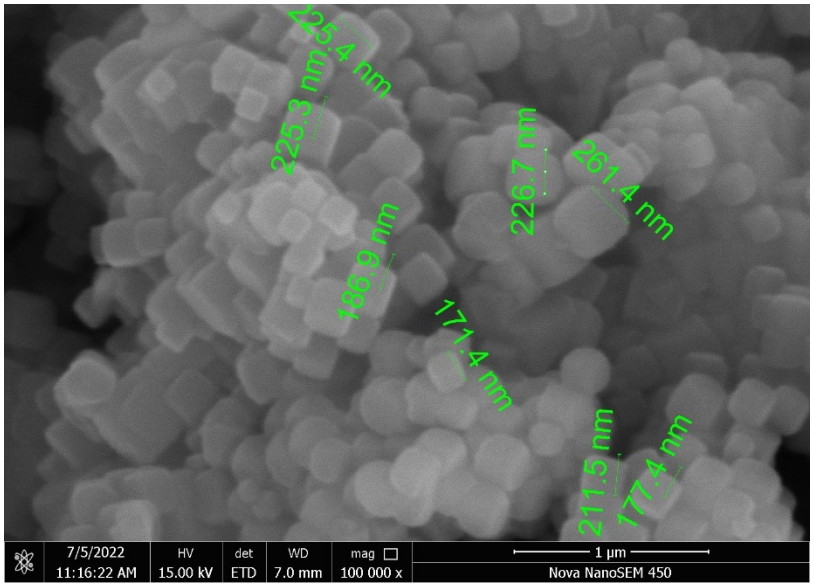

Figure S3. SEM images of FeCo-PBA@rGO/NF.

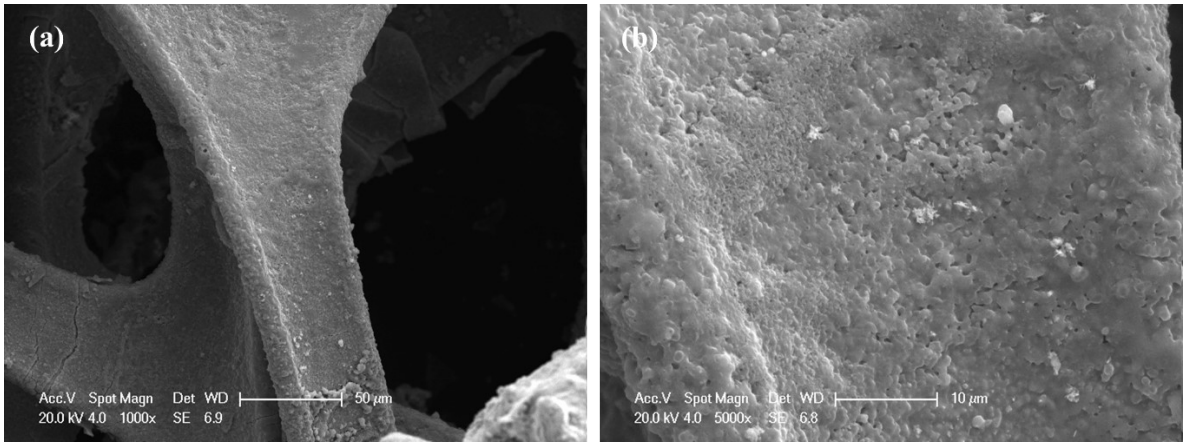

Figure S4. SEM images of FeCoP /NF.

Notes: In Figure S4, FeCoP/NF without rGO showed serious agglomeration, which proved that in-situ growth on rGO modified NF could fully and effectively promote the uniform dispersion of FeCo-PBA.[1]

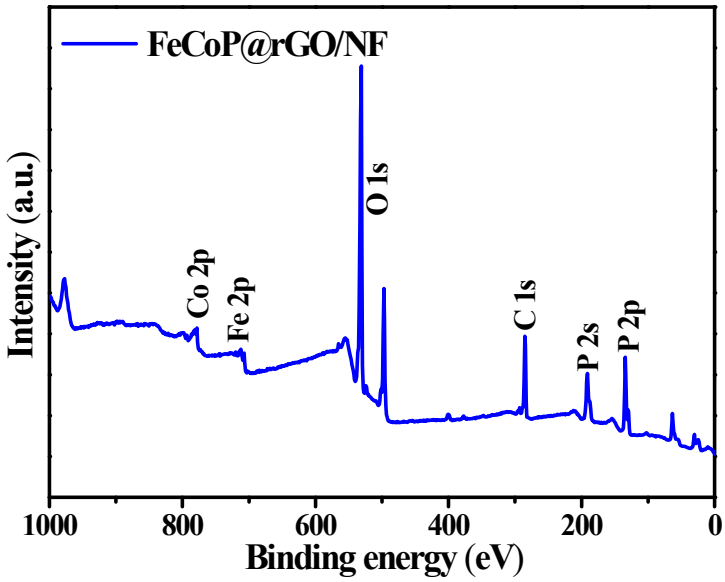

Figure S5. Full XPS spectrum of FeCoP@rGO/NF.

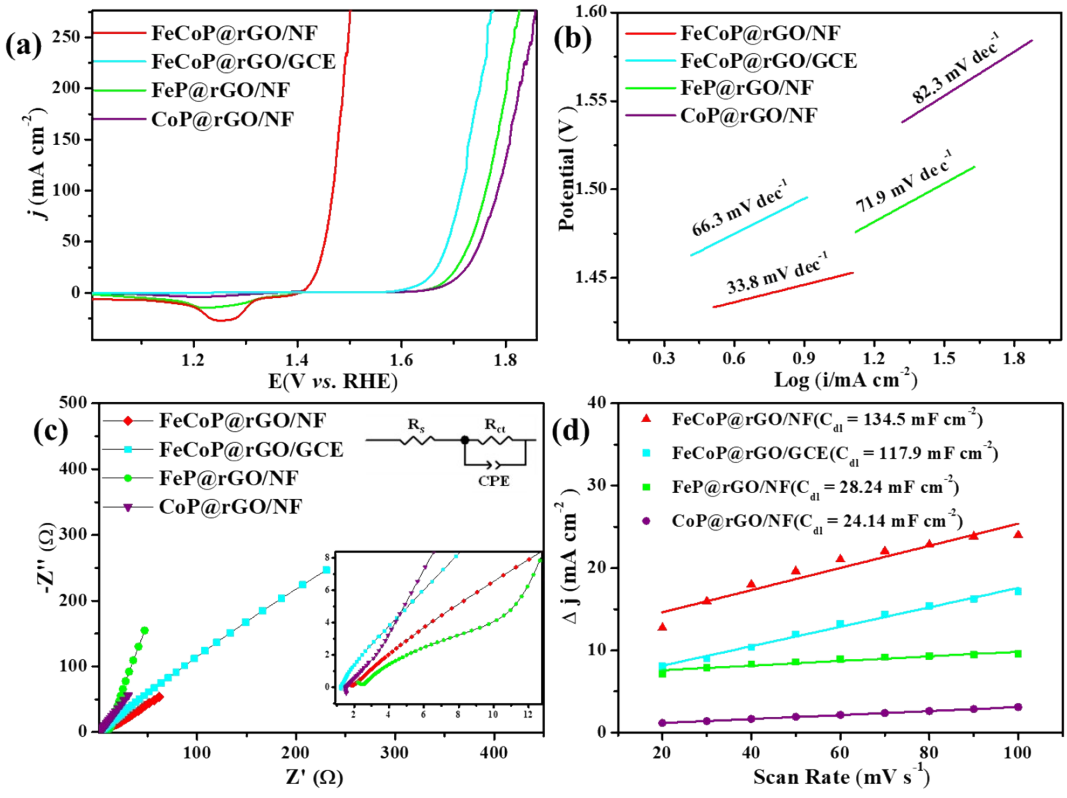

Figure S6. (a) OER polarization curves, (b) Tafel slopes, (c) Nyquist plots and (d) double layered capacity of FeCoP@rGO/NF, FeCoP@rGO/GCE, FeP@rGO/NF and CoP@rGO/NF in 1 M KOH.

Notes: From the Figure S6, it can be concluded that the OER activity of FeCoP@rGO in situ grown on NF support was much better than FeCoP@rGO powder without using nickel foam. The poor behavior of FeCoP@rGO powder may ascribe to the inevitable agglomeration in synthesizing process and the employment of polymer binder in electrode construction which would mask the active sites of the catalyst and slow down the electron transfer rate[2, 3]. Therefore, NF played a vital role in obtaining dispersed active materials, small reaction impedance, and accelerated proton transfer, effectively preventing catalyst from mechanically falling off.[4, 5]

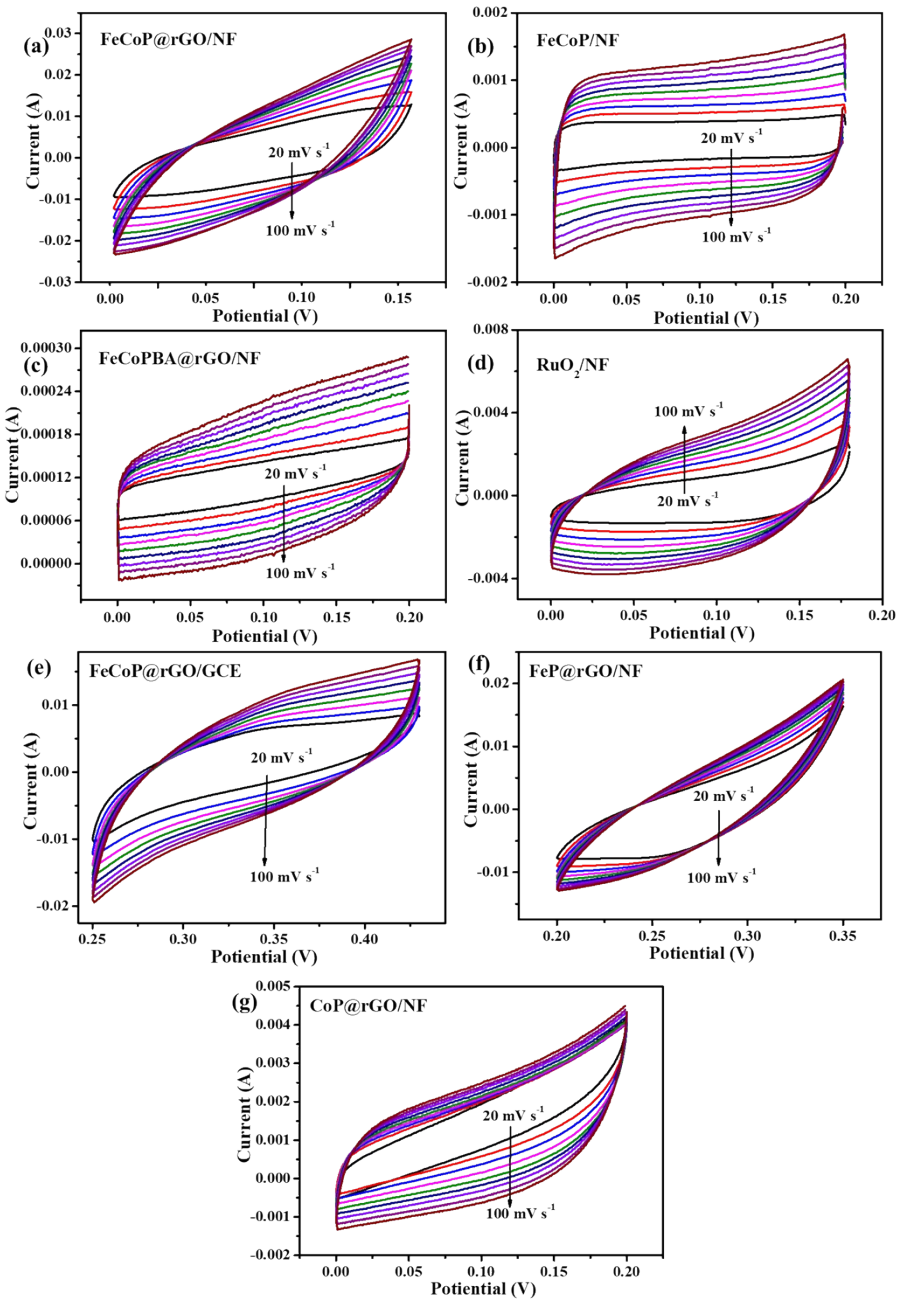

Figure S7. Cyclic voltammograms for (a) FeCoP@rGO/NF, (b) FeCoP/NF, (c) FeCo PBA@rGO/NF, (d) RuO_2/NF, (e) FeCoP@rGO/GCE, (f) FeP@rGO/NF and (g) CoP@rGO/NF at various scan rates of 20, 30, 40, 50, 60, 70, 80, 90, 100 mV s^{-1}.

Table S1. EIS equivalent circuit fitting results of FeCoP@rGO/NF, FeCoP/NF, FeCo-PBA@rGO/NF, RuO_2/NF, FeCoP@rGO/GCE, FeP@rGO/NF and CoP@rGO/NF.

Anodes	Rct (Ω)

FeCoP@rGO/NF	5.0
FeCoP/NF	90.6
FeCo-PBA@rGO/NF	102.8
RuO_2/NF	19.5
Blank NF	135.3
FeCoP@rGO/GCE	23.4
FeP@rGO/NF	109.3
CoP@rGO/NF	113.8

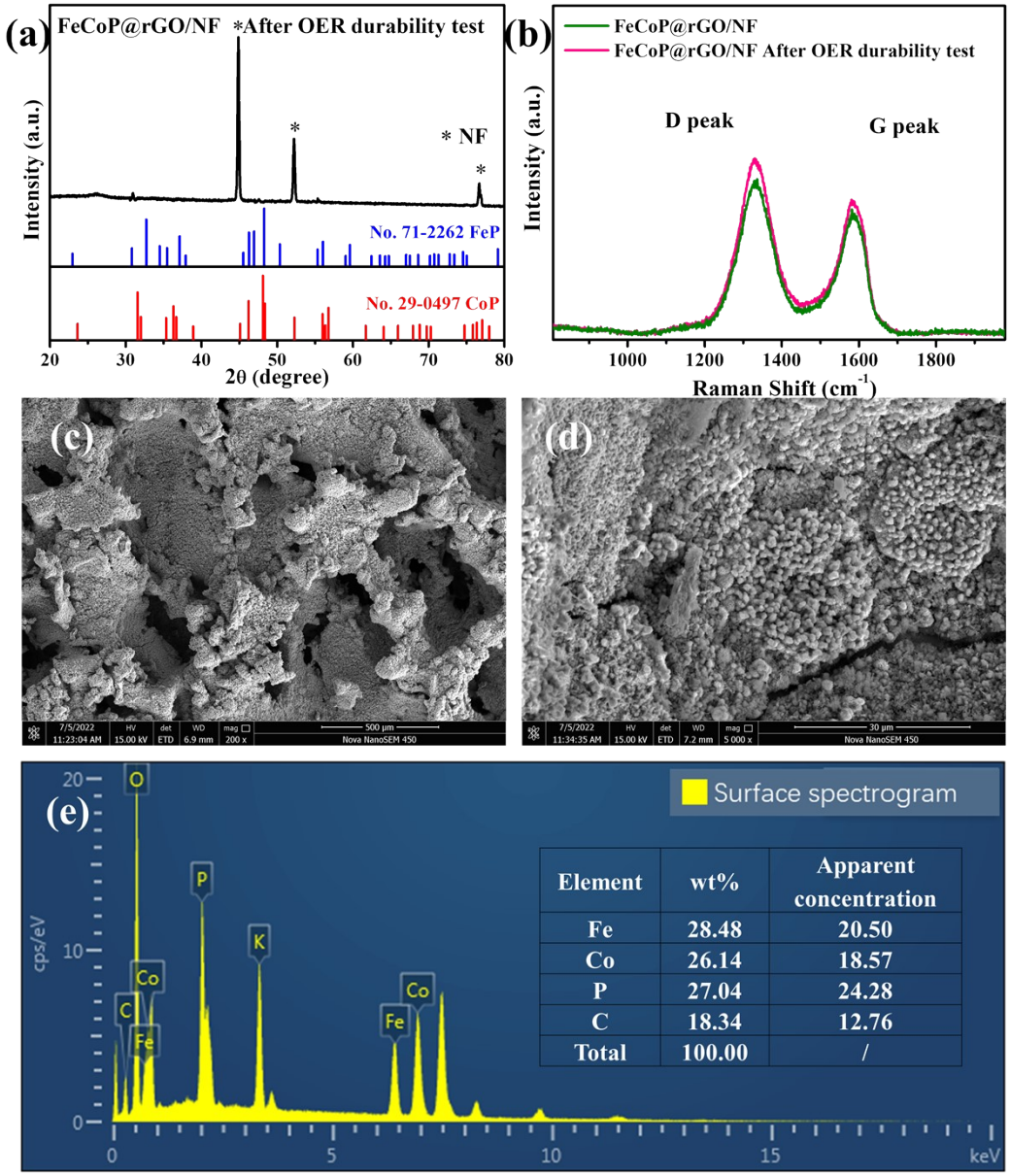

Element	wt%	Apparent concentration
Fe	28.48	20.50
Co	26.14	18.57
P	27.04	24.28
C	18.34	12.76
Total	100.00	/

Figure S8. (a) XRD, (b) Raman spectra, (c, d) SEM images and (e) EDX of FeCoP@rGO/NF after stability test.

Notes: After the OER durability test, the I_D/I_G value of FeCoP@rGO/NF obtained in Raman spectrum was 1.28, as low as the value before OER, which strongly proved that the rGO still combined firmly with NF after passing current and releasing gas.[6] Hence, it was proven that the strong graphene/nickel interaction played vital role in this satisfactory cyclic stability of FeCoP@rGO/NF.[7]

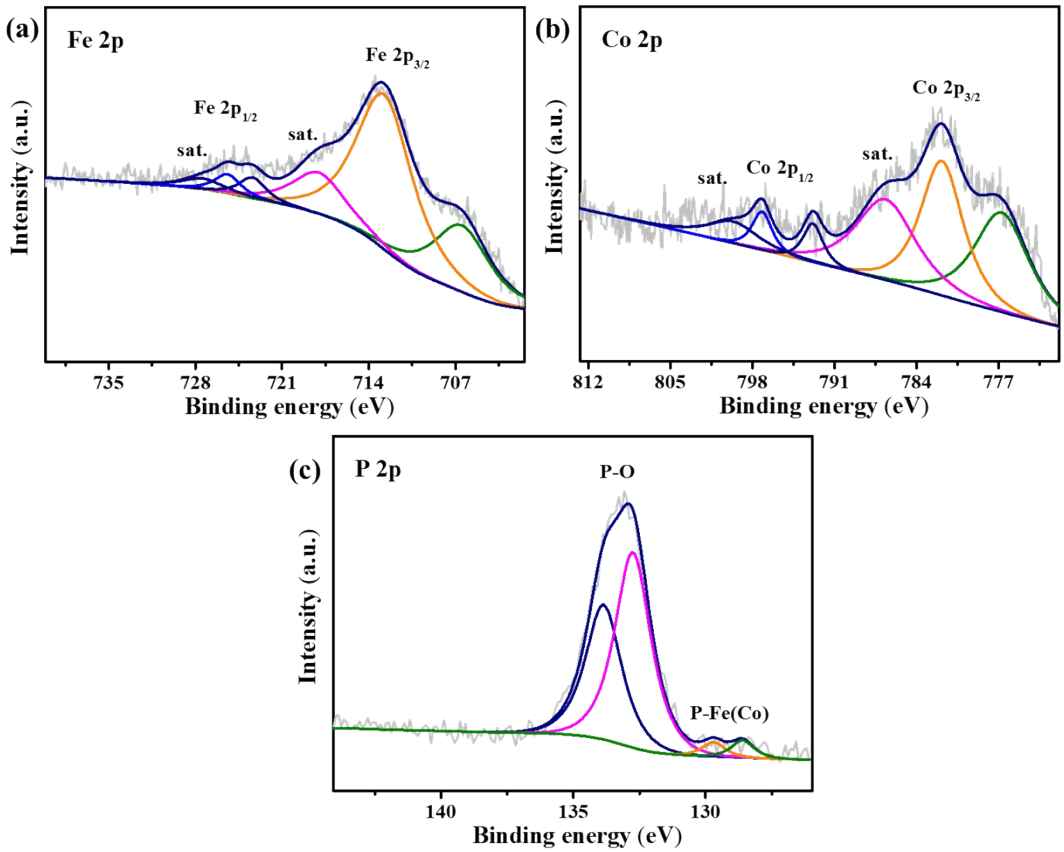

Figure S9. High-resolution XPS spectra of (a) Fe 2p, (b) Co 2p and (c) P 2p of FeCoP@rGO/NF after stability test.

Table S2. Comparison of OER performance between FeCoP@rGO/NF and several recently reported OER electrocatalysts in alkaline media.

Catalysts	Electrolyte	η_{10} (mV)	η_{100} (mV)	References
FeCoP@rGO/NF	1 M KOH	195	238	This work
	1 M KOH + seawater	217	262	
Fe_2O_3/NiO/NF	1 M KOH	182	219	[8]
$Ni_{0.8}Fe_{0.2}$-AHNAs	1 M KOH	190	230	[9]
S,P-(Ni,Mo,Fe)OOH/NiMoP /wood aerogel	1 M KOH + seawater	263(η_{50})	262	[10]
S-(Ni,Fe)OOH/NF	1 M KOH + seawater	229	300	[11]
FeP-Ni/NF	1 M KOH	-	294	[12]
NiFe/NiS_x/ NF	1 M KOH + 0.5 M NaCl	-	~290	[13]
$FeSe_2$@$CoSe_2$/rGO	1 M KOH	260	-	[14]
$Co_{0.9}Fe_{0.1}$-Se/NF	1 M KOH	246	-	[15]
CoS-FeS	1 M KOH	240	-	[16]

Table S3. Comparison of materials containing GO and NF.

Materials	Performance	
GO-coated NF	High mechanical strength and enhanced damping properties	17
CoFe-NC	ORR (half-wave potential 0.896 V) OER (η_{10} = 370 mV) Zn-air batteries (capacity 812.2 mAh g^{-1})	7
$NiFe_2O_4$@N/rGO	OER (η_{20} = 252 mV)	18
FeNi-NC	ORR (half-wave potential 0.89 V)	19
$FeNi_{0.25}$-NC	ORR (half-wave potential 0.86 V)	6
GO-Cu@Ni	High durability and stability	20
Ni_2P/RGO@NF	Overall water splitting 1.58 V	21
Co_3Fe_1-LDH/rGO/NF	OER (η_{10} = 250 mV)	22

Supporting References

1. X. L. Ren, Y. C. Tian, F. Shaik, J. N. Yang, R. Liu, K. M. Guo and B. Jiang, *Adv. Sustain. Syst.*, 2022, **6**, 13.
2. W. Liu, H. Liu, L. N. Dang, H. X. Zhang, X. L. Wu, B. Yang, Z. J. Li, X. W. Zhang, L. C. Lei and S. Jin, *Adv. Funct. Mater.*, 2017, **27**, 1603904.
3. S. S. Li, L. Wang, H. Su, A. N. Hong, Y. X. Wang, H. J. Yang, L. Ge, W. Y. Song, J. Liu, T. Y. Ma, X. H. Bu and P. Y. Feng, *Adv. Funct. Mater.*, 2022, **32**, 2200733
4. B. W. Zhou, J. W. Li, X. Zhang and J. X. Guo, *J. Alloys Compd.*, 2021, **862**, 158391.
5. H. Yang, M. Driess and P. W. Menezes, *Adv. Funct. Mater.*, 2021, **11**, 1614-6832.
6. J. Liu, C. H. Fan, G. B. Liu and L. H. Jiang, *Appl. Surf. Sci.*, 2021, **538**, 7.
7. Y. He, Z. W. Xi and C. L. Xu, *Nanotechnology*, 2022, **33**, 9.
8. L. Li, G. W. Zhang, B. Wang, D. L. Zhu, D. Liu, Y. Y. Liu and S. C. Yang, *ACS Appl. Mater. Interfaces*, 2021, **13**, 37152-37161.
9. C. W. Liang, P. C. Zou, A. Nairan, Y. Q. Zhang, J. X. Liu, K. W. Liu, S. Y. Hu, F. Y. Kang, H. J. Fan and C. Yang, *Energy Environ. Sci.*, 2020, **13**, 86-95.
10. H. J. Chen, Y. H. Zou, J. Li, K. W. Zhang, Y. Z. Xia, B. Hui and D. J. Yang, *Appl. Catal. B-Environ.*, 2021, **293**, 11.
11. L. Yu, L. B. Wu, B. McElhenny, S. W. Song, D. Luo, F. H. Zhang, Y. Yu, S. Chen and Z. F. Ren, *Energy Environ. Sci.*, 2020, **13**, 3439-3446.
12. G. Liu, Y. Wu, R. Yao, F. Zhao, Q. Zhao and J. P. Li, *Green Energy Environ.*, 2021, **6**, 496-505.
13. Y. Kuang, M. J. Kenney, Y. T. Meng, W. H. Hung, Y. J. Liu, J. E. Huang, R. Prasanna, P. S. Li, Y. P. Li, L. Wang, M. C. Lin, M. D. McGehee, X. M. Sun and H. J. Dai, *Proc. Natl. Acad. Sci. U. S. A.*, 2019, **116**, 6624-6629.
14. G. X. Zhu, X. L. Xie, X. Y. Li, Y. J. Liu, X. P. Shen, K. Q. Xu and S. W. Chen, *ACS Appl. Mater. Interfaces*, 2018, **10**, 19258-19270.
15. H. N. Ren, L. X. Yu, L. P. Yang, Z. H. Huang, F. Y. Kang and R. T. Lv, *J. Energy Chem.*, 2021, **60**, 194-201.
16. W. P. Wang, Y. Xu, J. L. Yao, X. E. Liu, Z. M. Yin and Z. C. Li, *Dalton Trans.*, 2020, **49**, 13352-13358.
17. H. Wang, C. Ma, W. Zhang, H. M. Cheng and Y. Zeng, *ACS Appl. Mater. Interfaces*, 2019, **11**, 42690-42696.
18. L. Cao, Z. Li, K. Su, M. Zhang and B. Cheng, *J. Energy Chem.*, 2021, **54**, 595-603.
19. U. Imtiaz, N. Iqbal, T. Noor, M. Z. Bin Amjad, M. A. Raza and A. Ali, *Int. J. Hydrog. Energy*, 2022, **47**, 37002-37012.
20. M. F. H. Othman, N. A. Rashidi, S. Yusup and T. Kida, 2020, **275**.
21. Z. H. Zhang, C. B. Li, H. R. Huang, J. F. Li, X. Q. Zhang, Z. Y. Li, H. Wei and H. B. Chu, *Electrochim. Acta*, 2020, **362**, 10.
22. J. W. Guo, Z. J. Wei, K. Wang and H. Zhang, *Int. J. Hydrog. Energy*, 2021, **46**, 27529-27542.